Supplementary information for "Optimal spin-charge interconversion in graphene through spin-pseudospin entanglement control"

Joaquín Medina Dueñas,[1,2,*] Santiago Giménez de Castro,[1] José H. García,[1,†] and Stephan Roche[1,3]

[1] *ICN2 — Catalan Institute of Nanoscience and Nanotechnology, CSIC and BIST, Campus UAB, Bellaterra 08193, Barcelona, Spain*
[2] *Department of Physics, Universitat Autònoma de Barcelona (UAB), Campus UAB, Bellaterra, 08193 Barcelona, Spain*
[3] *ICREA — Institució Catalana de Recerca i Estudis Avançats, 08010 Barcelona, Spain*

Supplementary Note 1. ELECTRONIC STRUCTURE: ANALYTICAL DEVELOPMENTS

We begin from the Hamiltonian in Eq. (1) of the main text. We transform the hamiltonian as $\mathcal{H}_{\boldsymbol{k}} \to U^\dagger \mathcal{H}_{\boldsymbol{k}} U$, with $U = \tau_+ + \tau_- \sigma_y$ and $\tau_\pm = (\tau_0 \pm \tau_z)/2$. Now the Hamiltonian at both valleys presents the same form, and we may focus our analysis only on the $\tau_z = +1$ subspace. We express the Hamiltonian in the basis $\{|-,+\rangle\,, |+,-\rangle\,, |-,-\rangle\,, |+,+\rangle\}$, where $|\mu,\xi\rangle$ corresponds to a pure state with pseudospin and spin respectively aligned along $\mu\hat{\boldsymbol{k}}$ and $\xi\hat{\boldsymbol{\varphi}} = \xi\hat{\boldsymbol{z}} \times \hat{\boldsymbol{k}}$, obtaining

$$\begin{aligned}\mathcal{H}_{\boldsymbol{k}} &= \begin{pmatrix} -\frac{1}{2}\lambda_{\mathrm{R}} - \hbar v_{\mathrm{gr}} k & -\frac{1}{2}(\lambda_{\mathrm{KM}} - \lambda_{\mathrm{R}}) & 0 & 0 \\ -\frac{1}{2}(\lambda_{\mathrm{KM}} - \lambda_{\mathrm{R}}) & -\frac{1}{2}\lambda_{\mathrm{R}} + \hbar v_{\mathrm{gr}} k & 0 & 0 \\ 0 & 0 & \frac{1}{2}\lambda_{\mathrm{R}} - \hbar v_{\mathrm{gr}} k & -\frac{1}{2}(\lambda_{\mathrm{KM}} + \lambda_{\mathrm{R}}) \\ 0 & 0 & -\frac{1}{2}(\lambda_{\mathrm{KM}} + \lambda_{\mathrm{R}}) & +\frac{1}{2}\lambda_{\mathrm{R}} + \hbar v_{\mathrm{gr}} k \end{pmatrix} \\ &= \bigoplus_{\chi=\mp} \mathcal{H}_{\boldsymbol{k},\chi}\ ,\end{aligned} \tag{S1}$$

with $\mathcal{H}_{\boldsymbol{k},\chi}$ given by Eq. (2) of the main text. Comparing with a simple gapped graphene model $\mathcal{H}_{\mathrm{gr}} = \hbar v_{\mathrm{gr}} \boldsymbol{k}\cdot\boldsymbol{\sigma} + \sigma_z \Delta/2$, we note that $\mathcal{H}_{\boldsymbol{k},\chi}$ corresponds to a Dirac cone with an effective mass of $\Delta_\chi = -(\lambda_{\mathrm{KM}} + \chi\lambda_{\mathrm{R}})$, with the additional feature of helical spin-pseudospin locking. The eigenvalues and eigenvectors of $\mathcal{H}_{\boldsymbol{k},\chi}$ are

$$E_{\chi,\pm} = \chi\frac{\lambda_{\mathrm{R}}}{2} \pm \varepsilon_\chi\ , \tag{S2a}$$

$$|E_{\chi,\pm}\rangle = \frac{1}{\sqrt{2\varepsilon_\chi}} \begin{pmatrix} -\mathrm{sign}(\Delta_\chi)\sqrt{\varepsilon_\chi \mp \hbar v_{\mathrm{gr}} k} \\ \pm\sqrt{\varepsilon_\chi \pm \hbar v_{\mathrm{gr}} k} \end{pmatrix}\ , \tag{S2b}$$

with $\varepsilon_\chi = [(\hbar v_{\mathrm{gr}} k)^2 + \Delta_\chi^2/4]^{1/2}$, and where $|E_{\chi,\pm}\rangle$ is represented in basis $\{|-,-\chi\rangle\,, |+,+\chi\rangle\}$, and we have omitted the $\boldsymbol{k}$ subindex for simplicity. The spin and pseudospin expectation values for the eigenstates are $\langle \boldsymbol{s}\rangle_{\chi,\pm} = \pm\chi\rho_\chi\hat{\boldsymbol{\varphi}}$ and $\langle\boldsymbol{\sigma}\rangle_{\chi,\pm} = \pm\rho_\chi\hat{\boldsymbol{k}}$, with $\rho_\chi = \hbar v_{\mathrm{gr}} k/\varepsilon_\chi$.

Even though the spin and pseudospin textures remain fully helical and radial, respectively, we find that these do not correspond to conserved quantities. Indeed, calculating the commutators we find

$$[\mathcal{H}\,,\, s_\varphi] = -\mathrm{i}\lambda_{\mathrm{R}}\sigma_\varphi s_z + \mathrm{i}\lambda_{\mathrm{KM}}\sigma_z s_k\ , \tag{S3a}$$

$$[\mathcal{H}\,,\, \sigma_k] = -\mathrm{i}\lambda_{\mathrm{KM}}\sigma_\varphi s_z + \mathrm{i}\lambda_{\mathrm{R}}\sigma_z s_k\ . \tag{S3b}$$

Additionally, we have $[\mathcal{H}, \sigma_z s_z] = -2\mathrm{i}\hbar v_{\mathrm{gr}} k\sigma_\varphi s_z$ and $[\mathcal{H}, \sigma_\varphi s_k] = 2\mathrm{i}\hbar v_{\mathrm{gr}} k\sigma_z s_k$, From this we obtain the conserved quantities,

$$\mathcal{Q}_1 = s_\varphi - \frac{1}{2\hbar v_{\mathrm{gr}} k}(\lambda_{\mathrm{R}}\sigma_z s_z + \lambda_{\mathrm{KM}}\sigma_\varphi s_k)\ , \tag{S4a}$$

$$\mathcal{Q}_2 = \sigma_k - \frac{1}{2\hbar v_{\mathrm{gr}} k}(\lambda_{\mathrm{KM}}\sigma_z s_z + \lambda_{\mathrm{R}}\sigma_\varphi s_k)\ , \tag{S4b}$$

along with $\mathcal{Q}_0 = \sigma_k s_\varphi$ already analysed in the main text.

We quantify entanglement using the concurrence, which is computed as follows. For a pair of coupled two-level systems, the concurrence is defined as $C_\psi = |\langle\psi|\sigma_y^{\mathrm{A}}\sigma_y^{\mathrm{B}}|\psi^*\rangle|$, where the quantisation axis within both subsystems is $\hat{\boldsymbol{z}}$, $\sigma_y^{\mathrm{A(B)}}$ is the Pauli matrix σ_y in subsystem A(B), and $|\psi^*\rangle$ is the complex conjugated wavefunction. We employ the same definition, but quantising the spin and pseudospin subspaces along $\hat{\boldsymbol{\varphi}}$ and $\hat{\boldsymbol{k}}$ respectively, where additionally we note that the eigenstates only present real coefficients as seen in Eq. (S2b). The concurrence for the eigenstates is thus $C_{\chi,\pm} = |\langle\sigma_\varphi s_k\rangle_{\chi,\pm}| = |\Delta_\chi|/2\varepsilon_\chi$. We note that $\langle\sigma_\varphi\rangle_{\chi,\pm} = \langle s_k\rangle_{\chi,\pm} = 0$, and thus $\langle\sigma_\varphi s_k\rangle_{\chi,\pm}$ reflects the non-separability of the wavefunction. Additionally, expressing $\sigma_z s_z$ as a rotation of $\sigma_\varphi s_k$, we obtain $\langle\sigma_z s_z\rangle_{\chi,\pm} = \chi\langle\sigma_\varphi s_k\rangle_{\chi,\pm}$. The conserved quantities can now be written as $\langle\mathcal{Q}_1\rangle_{\chi,\pm} = \langle s_\varphi\rangle_{\chi,\pm} - \Delta_\chi\langle\sigma_\varphi s_k\rangle_{\chi,\pm}/2\hbar v_{\mathrm{gr}}k$, and $\langle\mathcal{Q}_2\rangle_{\chi,\pm} = \langle\sigma_k\rangle_{\chi,\pm} - \chi\Delta_\chi\langle\sigma_\varphi s_k\rangle_{\chi,\pm}/2\hbar v_{\mathrm{gr}}k$. By these means, $\mathcal{Q}_1$ and $\mathcal{Q}_2$ are also interpreted as the interconversion of angular momentum from the individual spin and pseudospin projections to spin-pseudospin entanglement.

Supplementary Note 2. ELECTRONIC STRUCTURE: OTHER HAMILTONIAN TERMS

In real graphene-based heterostructures other proximity-induced interactions may also be relevant. We analyse the case of a staggered onsite potential and valley Zeeman SOC, which are relevant in graphene/TMD interfaces due to the breaking of sublattice symmetry [S1]; as well as the case of a Kekulé-O distortion which is relevant in graphene/topological insulator interfaces [S2]. These interactions are represented in the Hamiltonian by respectively including the terms $\mathcal{H}_{\mathrm{st}}$, $\mathcal{H}_{\mathrm{VZ}}$ and $\mathcal{H}_{\mathrm{Kek}}$, given by

$$\mathcal{H}_{\mathrm{st}} = \frac{1}{2}M\sigma_z \to \frac{1}{2}M\tau_z\sigma_z, \tag{S5a}$$

$$\mathcal{H}_{\mathrm{VZ}} = -\frac{1}{2}\lambda_{\mathrm{VZ}}\tau_z s_z \to -\frac{1}{2}\lambda_{\mathrm{VZ}}\tau_z s_z\ , \tag{S5b}$$

$$\mathcal{H}_{\mathrm{Kek}} = \Delta\tau_y\sigma_x \to \frac{1}{2}\Delta\tau_x\sigma_z\ , \tag{S5c}$$

where the right arrow indicates the unitary transformation U. We now consider the effects of these interactions for charge-to-spin conversion, calculated in the clean limit.

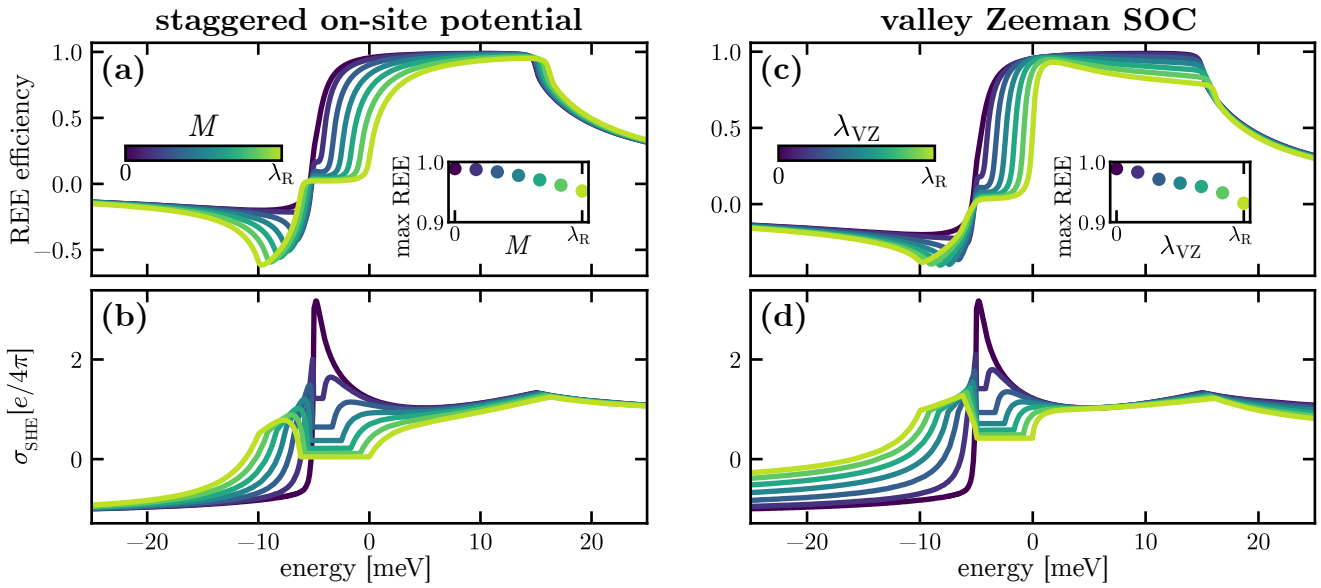

Supplementary Fig. 1. REE efficiency and spin Hall conductivity (σ^z_{xy}), including a staggered on-site potential $\mathcal{H}_{\mathrm{st}}$ and valley Zeeman SOC $\mathcal{H}_{\mathrm{VZ}}$. [$\lambda_{\mathrm{KM}} = \lambda_{\mathrm{R}} = 10\,\mathrm{meV}$]

The staggered potential introduces a hybridisation between the states $|-,\xi\rangle$ and $|+,\xi\rangle$ (for $\xi = \pm$), of opposite sign in each valley. At $k = 0$ a gap of magnitude $|M|$ opens between bands $E_{-,+}$ and E_{++} which brings both the pseudospin and spin textures out of the plane; while for larger momentum the interaction is suppressed due to the increasing spectral distance between the bands, and the textures approach the $M = 0$ case. Supplementary Fig. 1-(a, b) shows charge to spin conversion for different M values, with $\lambda_{\mathrm{KM}} = \lambda_{\mathrm{R}}$. We observe that the REE is more strongly suppressed at the low-energy end of the pseudogap, where the Fermi momentum is near $k = 0$, while at the high-energy end it is closer to the $M = 0$ case because the Fermi momentum is larger. The peak REE value is 0.952 for $M = \lambda_{\mathrm{R}}$, showing that the REE remains largely robust against a staggered on-site potential. In the SHE, shown in panel (b), the gap opening regularises the diverging peak at $k = 0$, where a finite SHE appears within the gap and tends to zero for increasing M, as the gap is dominated by the topologically trivial staggered potential.

Valley Zeeman SOC, on the other hand, introduces a hybridisation between states of the same pseudospin and opposite spin polarisations, $|\mu,+\rangle$ and $|\mu,-\rangle$ (for $\mu = \pm$). The spectral distance between these states remains fairly constant throughout the spectrum, and thus the interaction is not suppressed at large momentum. The eigenstates acquire a finite out-of-plane spin texture component which suppresses Rashba-related effects, as can be seen by the reduction of the asymptotic SHE value, and the REE at the high-energy end of the pseudogap, shown in Supplementary Fig. 1-(d) and (c), respectively. At $k = 0$ the gap opening regularises the diverging peak in the SHE, similar to the case of the staggered potential. The REE, on the contrary, reaches its peak value near the low-energy end of the pseudogap, where the out-of-plane component of the spin texture is zero. For $\lambda_{\mathrm{VZ}} = \lambda_{\mathrm{R}}$ the peak REE value is of 0.932, also showing robustness against valley Zeeman SOC.

For the Kekulé-O distortion we note that under a π rotation about τ_y, $\mathcal{H}_{\mathrm{Kek}}$ takes the same form as $\mathcal{H}_{\mathrm{st}}$, while the rest of the Hamiltonian terms remain unaffected. The Kekulé-O distortion thus presents the same effects as the staggered on-site potential, where the eigenstates are valley-polarised along τ_x rather than τ_z.

Supplementary Note 3. RASHBA-EDELSTEIN EFFECT AT FINITE TEMPERATURE

We perform the calculations for the REE within the constant broadening approximation considering a finite temperature, which only affects the carrier distribution.The corresponding longitudinal current J_x and non-equilibrium spin density S_y correspond to convolutions of the zero temperature result with the derivative of the Fermi-Dirac distribution, as indicated by Eq. (7a) of the main text. For the transport velocity, we recall that it is defined based on the Einstein relation, and therefore the density of states appearing therein (see Methods section in the main text) must also be convoluted by the Fermi-Dirac distribution derivative in order to reflect the amount of carriers available for transport [S3]. The results for the REE efficiency are shown in Supplementary Fig. 2. We observe that the REE efficiency in the optimal $\lambda_{\mathrm{KM}} = \lambda_{\mathrm{R}}$ case maintains its peak value up to $\sim 30\,\mathrm{K}$, whereas for the $\lambda_{\mathrm{KM}} = 0$ case the peak REE efficiency is reduced for any finite temperature. We conclude that the system is in general sensitive to thermal effects due to the small size of the Rashba pseudogap, where the proposed spin-charge-interconversion phenomena are most relevant. Nevertheless, in the optimal case we propose, the plateau-shaped maximum grants further robustness to the REE against the effects of finite temperature. We also compute the spin Hall conductivity in this case, shown in Supplementary Fig. R1-(c, d), where we observe a similar behaviour. For $\lambda_{\mathrm{KM}} = \lambda_{\mathrm{R}}$, the SHE conductivity is finite and presents the same sign throughout the entire pseudogap, which grants a further robustness against the thermal spreading of the electron occupation.

Supplementary Note 4. TRANSPORT CALCULATIONS: COMPLETE DATA

Supplementary Fig. 3 shows the results for the real-space simulations for $\lambda_{\mathrm{KM}}/\lambda_{\mathrm{R}} = 0, \frac{1}{2}$ and 1 including disorder. These results were obtained in a system of 529 million unit cells by the KPM method, using a Chebyshev expansion leading to a numerical Jackson broadening of 0.5 meV at the band centre. We observe a decrease in the relaxation time τ due to the effects of disorder scattering, as observed by the decrease of the Fermi surface responses σ_{xx} and χ_{yx}; while the REE efficiency remains largely robust. We also include the electron mobility calculations which allow to compare with experimental graphene samples, showing that the disorder values here explored compare reasonably to real graphene samples of medium to good quality [S4, S5]. Here, a charge density of $10^{12}\,\mathrm{cm}^{-2}$ is achieved at a Fermi level of approximately $\pm 100\,\mathrm{meV}$ with respect to charge neutrality.

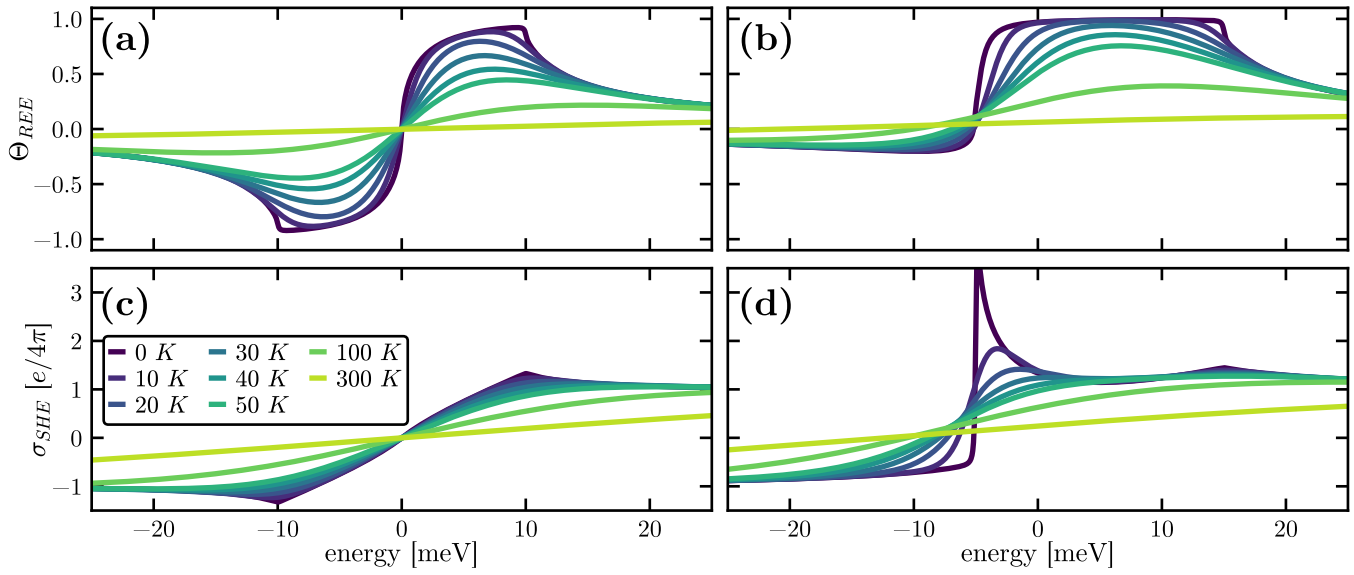

Supplementary Fig. 2. REE efficiency (a, b) and SHE conductivity (c, d) at finite temperature for $\lambda_{\mathrm{KM}} = 0$ (a, c) and $\lambda_{\mathrm{KM}} = \lambda_{\mathrm{R}}$ (b, d).

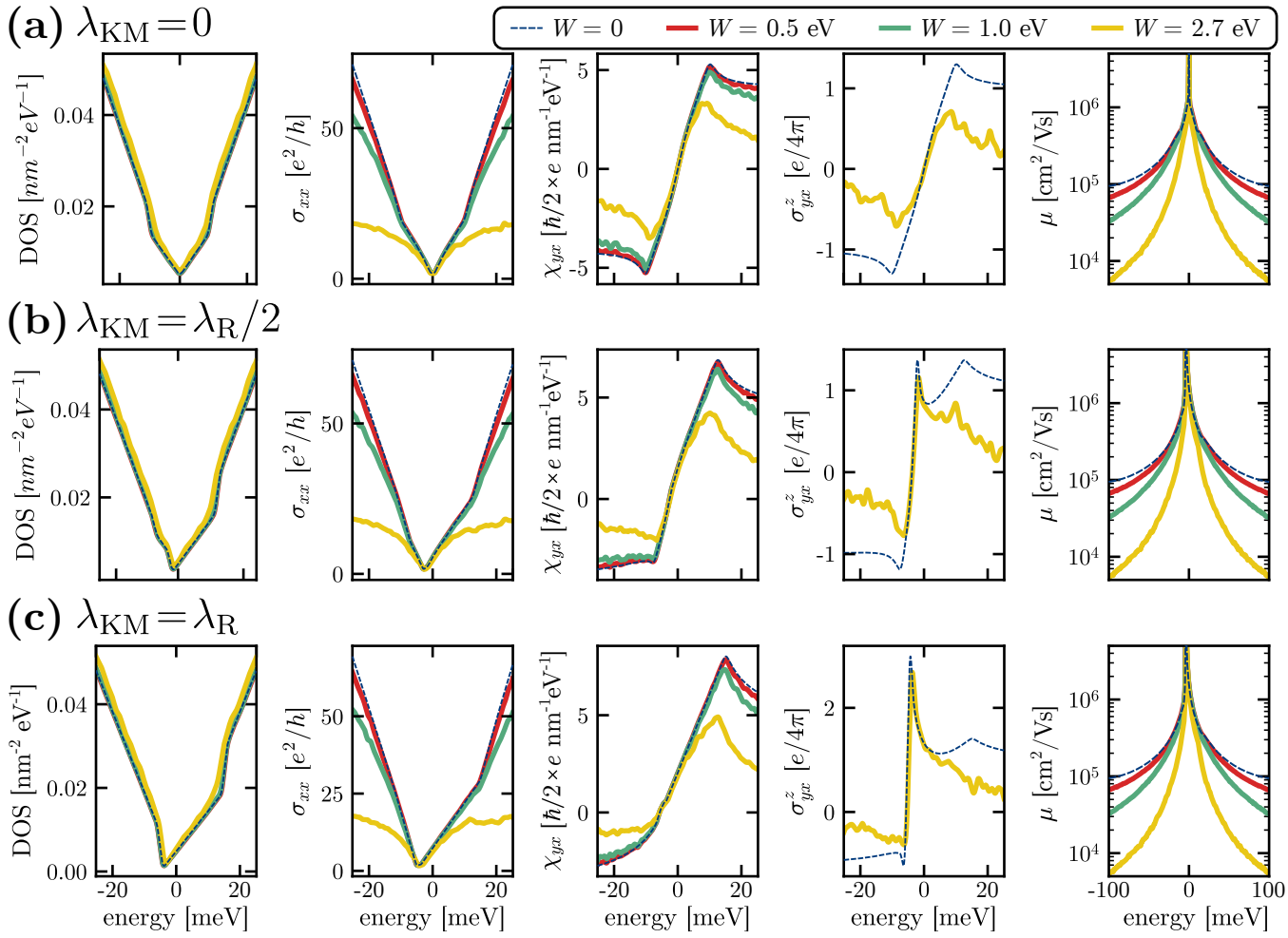

Supplementary Fig. 3. Results of KPM simulations of disordered systems (density of states, longitudinal conductivity, REE spin density, and SHE conductivity) and charge mobility. [$\lambda_{\mathrm{R}} = 10\,\mathrm{meV}$]

* Corresponding Author joaquin.medina@icn2.cat
† Corresponding Author josehugo.garcia@icn2.cat

[S1] Martin Gmitra and Jaroslav Fabian, "Graphene on transition-metal dichalcogenides: A platform for proximity spin-orbit physics and optospintronics," Phys. Rev. B **92**, 155403 (2015).
[S2] Kenan Song, David Soriano, Aron W. Cummings, Roberto Robles, Pablo Ordejón, and Stephan Roche, "Spin proximity effects in graphene/topological insulator heterostructures," Nano Letters **18**, 2033–2039 (2018).
[S3] Massimiliano Di Ventra, *Electrical Transport in Nanoscale Systems* (Cambridge University Press, 2008).
[S4] Luis E. F. Foa Torres, Stephan Roche, and Jean-Christophe Charlier, *Introduction to Graphene-Based Nanomaterials: From Electronic Structure to Quantum Transport* (Cambridge University Press, Cambridge, England, 2020).
[S5] Y.-W. Tan, Y. Zhang, K. Bolotin, Y. Zhao, S. Adam, E. H. Hwang, S. Das Sarma, H. L. Stormer, and P. Kim, "Measurement of scattering rate and minimum conductivity in graphene," Physical Review Letters **99** (2007), 10.1103/physrevlett.99.246803.